



Stabilization of anionic and neutral forms of a fluorophoric ligand at the active site of human carbonic anhydrase I

Sumathra Manokaran^a, Jayati Banerjee^b, Sanku Mallik^b, D.K. Srivastava^{a,*}

^a Department of Chemistry and Biochemistry, North Dakota State University, Fargo, ND 58105, USA

^b Department of Pharmaceutical Sciences, North Dakota State University, Fargo, ND 58105, USA

ARTICLE INFO

Article history:

Received 9 December 2009

Received in revised form 23 June 2010

Accepted 25 June 2010

Available online 8 July 2010

Keywords:

Human carbonic anhydrase-I

Inhibitor design

Sulfonamide

Fluorophore

Dansylamide

Ligand binding

ABSTRACT

We synthesized a fluorogenic dansylamide derivative (JB2-48), which fills the entire (15 Å deep) active site pocket of human carbonic anhydrase I, and investigated the contributions of sulfonamide and hydrophobic regions of the ligand structure on the spectral, kinetic, and thermodynamic properties of the enzyme–ligand complex. The steady-state and fluorescence lifetime data revealed that the deprotonation of the sulfonamide moiety of the enzyme bound ligand increases the fluorescence emission intensity as well as the lifetime of the fluorophores. This is manifested via the electrostatic interaction between the active site resident Zn²⁺ cofactor and the negatively charged sulfonamide group of the ligand, and such interaction contributes to about 2.2 kcal/mol ($\Delta\Delta G^\circ$) and 0.89 kcal/mol ($\Delta\Delta G^\ddagger$) energy in stabilizing the ground and the putative transition states, respectively. We provide evidence that the anionic and neutral forms of JB2-48 are stabilized by the complementary microscopic/conformational states of the enzyme. The implication of the mechanistic studies presented herein in rationale design of carbonic anhydrase inhibitors is discussed.

© 2010 Elsevier B.V. All rights reserved.

1. Introduction

Although enzymes are evolved to catalyze specific biological reactions, their active site pockets appear to lack absolute discriminatory features between their cognate physiological substrates/products and a wide range of structurally diverse compounds (which exhibit no structural resemblance to putative substrates, products, or intermediates of enzyme catalyzed reactions) [1–3]. The ability of enzymes to accommodate structurally diverse ligands (due to the marked dynamic flexibility) within their active site pockets have led to designing a variety of therapeutic agents against pathogenic enzymes [4–6]. Given this, it is conceivable that the X-ray crystallographic structure of an enzyme bound inhibitor may not serve as an ideal template for predictably designing highly potent enzyme inhibitors as potential drugs [7–9].

Of 15 different isozymes of carbonic anhydrases (CAs; EC 4.2.1.1), which are ubiquitously distributed zinc metalloproteins, and are involved in a variety of physiological functions, carbonic anhydrase I (hCA I) is representative of one of the cytosolic enzymes, which is present in all animal kingdom [10–17]. Although different isozymes of carbonic anhydrases have been found to be inhibited by a variety of differently functionalized ligands, aryl sulfonamides serve as repre-

sentative potent inhibitors of these enzymes [10,13–15]. The X-ray crystallographic structures of several CA-isozymes in the presence of different aryl sulfonamide inhibitors have been solved to atomic resolutions [17–23]. Both crystallographic as well as NMR data reveal that the sulfonamide moieties of the ligands interact with active site resident Zn²⁺ cofactor as well as with Thr-199 [13,14,22,24–29]. The structural data further suggest that the active site Zn²⁺ electrostatically interacts with the negatively charged nitrogen (produced via deprotonation of the amide group) of sulfonamide moiety of the ligand [25–28].

Since the aliphatic sulfonamides do not serve as potent inhibitors of carbonic anhydrases [13,30], it follows that the wide active site pocket of the enzyme needs to be occupied by bulky (viz., aromatic) groups of the ligand structures. Based on the structure-activity relationship, it has been apparent that both sulfonamide and aromatic moieties of ligands contribute to the overall binding energy of carbonic anhydrase–ligand complexes [31–33]. However, to the best of our knowledge, no systematic studies have been conducted to assess the contributions of hydrophobic and electrostatic interactions of ligand structures in stabilizing the corresponding enzyme–ligand complexes. This issue is specifically addressed in this manuscript.

We recently investigated the detailed microscopic pathways for the binding of dansylamide to hCA I versus hCA II, and provided evidence that despite a marked structural similarity, the active site pockets of these enzymes behave differently in accommodating the common ligand [34]. However, one of the deficiencies of dansylamide fluorophore has been the comparable quantum yields of its aqueous

Abbreviations: CA, Carbonic anhydrase; CA-I, human carbonic anhydrase I; hCA-II, human carbonic anhydrase II; EDTA, Ethylenediaminetetraacetic acid; DMSO, Dimethylsulfoxide

* Corresponding author. Tel.: +1 701 231 7831; fax: +1 701 231 7884.

E-mail address: dk.srivastava@ndsu.edu (D.K. Srivastava).

versus the enzyme bound forms, and thus it did not serve as an ideal ligand for pursuing detailed mechanistic studies such as reported herein [35]. Although a few other fluorescent probes for carbonic anhydrases have been reported in the literature, they have not been utilized toward the above goal presumably due to their challenging synthetic protocols [36,37]. Given these, we synthesized a series of conjugated fluorophores using dansylamide as the parent compound [38], of which JB2-48 was deemed to be an ideal fluorophores for delineating the contributions of sulfonamide and hydrophobic regions in binding with hCA I using the fluorescence signals of the enzyme–ligand complex.

2. Experimental procedures

2.1. Materials

Zinc sulfate, ampicillin, chloramphenicol and IPTG were purchased from Life Science Resources, Milwaukee, WI; yeast extracts, and tryptone were purchased from Becton Dickinson, Sparks, MD; Acetonitrile was from Aldrich Chemicals, Milwaukee, WI; HEPES, p-aminomethylbenzenesulfonamide-agarose, p-nitrophenyl acetate and PMSF were obtained from Sigma; All the chemicals needed for synthesis of JB2-48 were purchased from Aldrich Chemical Company, Milwaukee, WI. The E. coli expression system BL21codon plus DE3(RIL) was from Stratagene, La Jolla, CA. All other chemicals were of reagent grade, and were used without further purification.

2.2. Methods

The compound JB2-48 was synthesized as described by Banerjee et al. [38]. The recombinant form of human carbonic anhydrase I (hCA I) was cloned, expressed and purified as per the previously developed protocol in our lab [34]. All experiments were performed in 25 mM HEPES buffer, pH 7.0, containing 10% DMSO (the standard buffer). Following buffers, containing 10% DMSO, were used for the pH-dependent experiments. pH 5.0: 25 mM acetate buffer; pH 6.0–6.5: 25 mM MES buffer; pH 7.0–7.5: 25 mM HEPES buffer, pH 8.0–9.0: 25 mM Tris-phosphate buffer.

2.2.1. Steady-state spectrofluorometric studies

All steady-state spectrofluorometric studies involving dansylamide derivative, JB2-48, were performed on a Perkin Elmer lambda 50-B spectrofluorometer, equipped with a magnetic stirrer and thermostated water bath. The stock solution of JB2-48 was prepared in 100% DMSO and was diluted in 25 mM HEPES buffer, pH 7.0, containing 10% DMSO during the course of the titration as well as kinetic experiments. The emission spectra of JB2-48 in the absence and presence of hCA I was acquired by fixing the excitation wavelength at 336 nm. The contributions of Raman/Rayleigh scattering from the emission spectra of fluorophores were eliminated by subtracting the spectra of the buffer (obtained under identical experimental conditions). The dissociation constant of the hCA I–JB2-48 complex was determined by titrating a fixed concentration of the enzyme (2 μ M) with increasing concentrations of the ligand in the standard HEPES buffer containing 10% DMSO, pH 7.0. The excitation and emission slits were 9 mm each. The decrease in fluorescence emission intensity of the protein and the increase in the fluorescence emission intensity of probe were monitored at 330 nm and 470 nm, respectively ($\lambda_{\text{ex}} = 280$ nm). The dissociation constant of the hCA I–JB2-48 complex was determined by analyzing the binding isotherm by Eq. (1) as elaborated by Qin and Srivastava [39].

$$\Delta F = \Delta F_{\text{max}} * \left\{ \frac{(E_t * n + L_t + K_d) - \sqrt{(E_t * n + L_t + K_d)^2 - 4E_t * n * L_t}}{2} \right\} \quad (1)$$

Where ΔF and ΔF_{max} are observed and maximum fluorescence changes for the binding of JB2-48 to hCA I, respectively. E_t , L_t , n , and K_d

are total enzyme (hCA I), total ligand (JB2-48), stoichiometry of the enzyme–ligand complex and the dissociation constant of the enzyme–ligand complex, respectively.

2.2.2. Fluorescence Lifetime measurements

Fluorescence Lifetime measurements were performed on a custom designed Photon Technology International (PTI) Fluorescence-Lifetime Instrument. The excitation sources for measuring the time resolved fluorescence decay were the Light Emitting diodes (LEDs) with maximum power outputs at 280 nm and 340 nm, respectively. Whereas the 280 nm LED was utilized to excite the intrinsic fluorescence of the protein (primarily contributed by the tryptophan residues), the 340 nm LED was utilized to excite JB2-48 fluorescent probe. The emitted light was detected (at right angle of the excitation source) by means of a stroboscopic emission monochromator configured at an appropriate wavelength. The time resolved fluorescence decay curves were analyzed to obtain the lifetimes of the fluorophores under different conditions by the aid of the PTI's software, Felix 32.

2.2.3. Steady state kinetics and spectrophotometric Studies

All spectrophotometric studies were performed on the Molecular Devices SpectraMax Plus microplate reader, equipped with a cuvette holder and magnetic stirrer. The enzyme activity of hCA I was determined by monitoring the hydrolysis of p-nitrophenyl acetate substrate at 348 nm in 25 mM HEPES buffer, pH 7.0, containing 10% DMSO. The K_i for JB2-48 was determined as described by Banerjee et al. [42].

The pK_a values of free JB2-48 were determined by monitoring the increase in absorption of the compound at 336 nm as a function of the increasing pH value.

2.2.4. Transient kinetic experiments

Transient kinetic experiments were performed on an Applied Photophysics SX-18 MV stopped-flow system, equipped with both absorption and fluorescence detecting photomultiplier tubes. The dead time of stopped flow was 1.3 ms. For fluorescence measurement, the light path was configured such that the fluorescence photomultiplier detected the emitting light via the 2-mm path length. The excitation wavelength was maintained at 336 nm, and a 395-nm cut-off filter was installed at the exit port of the cuvette to measure the time dependent changes in the fluorescence intensity by a photomultiplier tube. The stopped flow traces were analyzed by the data analysis package provided by Applied Photophysics.

2.2.5. pH Jump Relaxation Studies

These experiments were performed by mixing a solution of the hCA I–JB2-48 complex, maintained at one pH, with a concentrated buffer at the other pH in the stopped-flow syringes, and recording the fluorescence change as described above. For a low to high pH jump, syringe A contained 2 μ M hCA I + 20 μ M JB2-48 in 5 mM Acetate buffer at pH 5.0 containing 10% DMSO and syringe B contained 200 mM Tris at pH 9.0 with 10% DMSO. Upon mixing, the pH of the solution changed to be pH 9.0. For a high to low pH jump experiment, syringe A contained 2 μ M hCA I + 20 μ M JB2-48 in 5 mM Tris at pH 9.0 having 10% DMSO and syringe B contained 200 mM Acetate buffer at pH 5 with 10% DMSO. Upon mixing, the pH of the mixture changed to 5.0.

2.2.6. Molecular modeling studies

The molecular modeling studies were performed on a Silicon Graphics-O2 molecular modeling workstation with the aid of Accelrys software, InsightII(98). The coordinates for the X-ray crystallographic structures of bovine CA II complexed with dansylamide (1okl.pdb) and hCA I complexed with acetazolamide (1azm.pdb) were downloaded from Research Collaboratory for Structural Bioinformatics

(RCSB) Protein Data Bank. The backbones of these proteins were superimposed, and the dansylamide was computationally transferred from bovine CA II to hCA I. The structure of JB2-48 was built on the backbone of the enzyme bound dansylamide with the aid of the software Builder under the InsightII(98) platform.

3. Results

We synthesized JB2-48 as a fluorescent ligand for hCA I by conjugating p-hydroxybenzaldehyde with p-aminonaphthalein sulfonamide [38] as outlined in the scheme of Fig. 1. The molecular modeling data revealed that unlike its parent compound, dansylamide (which occupied only 1/3 of the enzyme's active site pocket), JB2-48 filled nearly the entire (~15 Å deep) hydrophobic pocket of hCA I (Fig. 1). Hence, JB2-48 could be envisaged to experience “full” hydrophobicity of the enzyme's active site environment. We observed that both free as well as the enzyme bound form of JB2-48 was fairly stable at the room temperature, and showed no evidence of degradation/hydrolysis during the course of any of the experiments reported herein. We further observed that 10% DMSO had no influence on the catalytic activity of the enzyme, and the enzyme was stable at different pH values during the course of all experiments reported herein (data not shown).

In a preliminary manner, we previously noted that the excitation and emission maxima of free JB2-48 were 336 nm and 528 nm, respectively, and that the emission maximum was blue shifted to 470 nm (with concomitant increase in the fluorescence intensity) upon binding to hCA I [38]. This is in contrast to the emission maximum of the enzyme-bound dansylamide as being equal to 458 nm [34]. In addition, the quantum yield of the enzyme bound JB2-48 (as compared to the free ligand) is increased by about 40 fold [38], and this feature allowed us to easily differentiate between the free versus enzyme bound form of the ligand via spectrofluorometric and transient kinetic approaches (see below).

We performed fluorescence spectroscopic studies of the above species as a function of pH of the buffer medium (Fig. 2A). The inset of Fig. 2A shows the representative fluorescence emission spectra ($\lambda_{\text{ex}} = 336 \text{ nm}$) of the enzyme bound JB2-48 at pH 5.0 and 9.0. We confirmed that at these pH extrema, the catalytic activity of the enzyme remains unaffected during the time regime of all spectral,

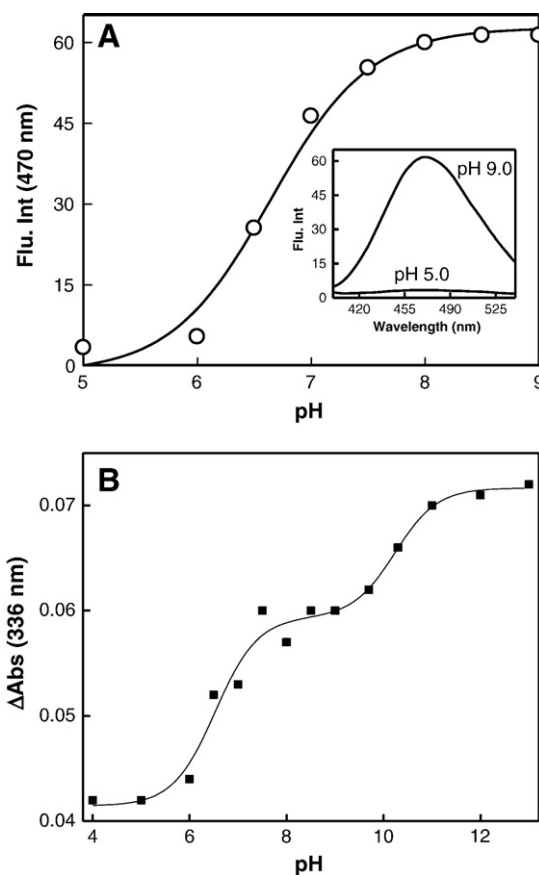


Fig. 2. pH-dependent changes in the fluorescence emission profile of JB2-48 in the presence (panel A) and absence (Panel B) of hCA I. The main figure of Panel A shows the increase in fluorescence emission intensity of the enzyme bound JB2-48 ($\lambda_{\text{ex}} = 336 \text{ nm}$, $\lambda_{\text{em}} = 470 \text{ nm}$) as a function of pH. [hCA I] = 10 μM , [JB2-48] = 3 μM . The solid line is the best fit of the data according to the Henderson–Hasselbalch equation for the pK_a value of 6.6 ± 0.1 . The inset shows the representative emission spectra ($\lambda_{\text{ex}} = 336 \text{ nm}$) of the enzyme bound JB2-48 complex at pH 5.0 and 9.0. Panel B shows the increase in absorption (at 336 nm) of aqueous solution of JB2-48 solution as a function of pH. The solid smooth line is the best fit of the data according to the Henderson–Hasselbalch equation for two pK_a values of 6.5 and 10.2, respectively.

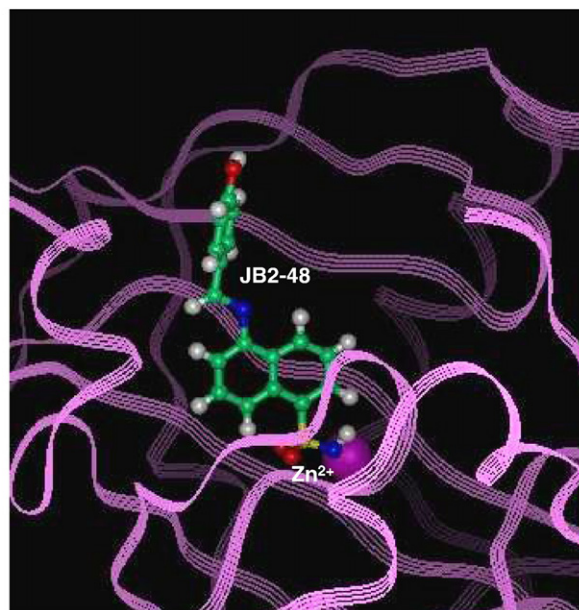
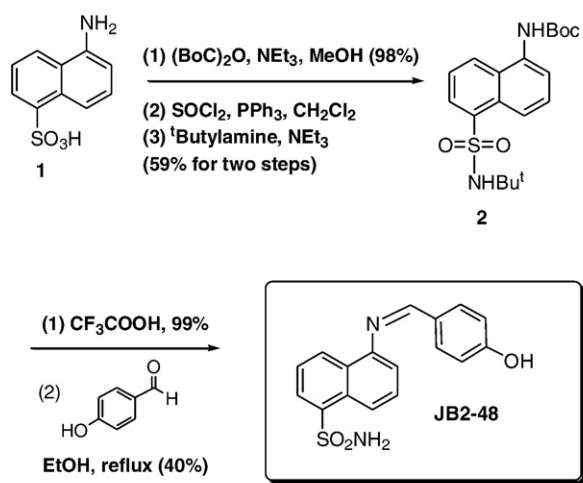


Fig. 1. Synthetic scheme of JB2-48 and the molecular model for its occupancy at the active site pocket of hCA I.

kinetic, and thermodynamic studies reported in this as well as in subsequent sections. The data of Fig. 2A reveal that the fluorescence emission intensity of the enzyme bound JB2-48 at pH 5.0 is significantly lower than that observed at pH 9.0. The main panel of Fig. 2A shows the pH dependent changes in the fluorescence emission intensity of the enzyme–JB2-48 complex. The solid smooth line is the best fit of the data according to the Henderson–Hasselbalch equation for the pK_a value of 6.6. The latter value is similar to the pK_a derived from the pH dependent changes in the binding affinity of dansylamide with hCA I ($pK_a = 6.3$) and hCA II ($pK_a = 6.4$) [34].

Since JB2-48 contains two ionizable groups (viz., the sulfonamide group of the naphthalene ring and the phenolic hydroxyl group), we proceeded to determine their pK_a values using free fluorophore. In this endeavor, we noted that the absorption maximum of JB2-48 increases at 336 nm as a function of the pH of the solution. Using the above signal, we titrated a fixed concentration of JB2-48 (3 μM) with increasing aliquots of dilute NaOH and recorded the resultant pH value (Fig. 2B). The data were analyzed according to the Henderson–Hasselbalch equation (solid smooth line) for two pK_a values of 6.5 and 10.2, respectively. Given that the pK_a value of sulfonamide group in “aqueous” benzenesulfonamide is 9.79 [35], we ascribe our experimentally determined pK_a 's of 6.5 and 10.2 (Fig. 2B) to the phenolic hydroxyl group and the sulfonamide moiety of JB2-48, respectively. On comparison of the titration results of Fig. 2A and B, it appears evident that the coordination of sulfonamide group of JB2-48 with the active site resident Zn^{2+} of hCA I (forming a Lewis acid–base pair) decreases its pK_a value by about 3 units. This is in accord with the wide spread view that at neutral pH, the Zn^{2+} cofactor electrostatically interacts with the negatively charged nitrogen of aryl sulfonamide ligands in different isoforms of carbonic anhydrases [24–28]. Although the above coordination is also likely to decrease the pK_a value of the phenolic hydroxyl group of JB2-48 (due to an extended conjugation in the entire molecule), we could not reliably ascertain its magnitude. However, such a decrease is unlikely to be significant since the enzyme bound form of JB2-48 yields only one pK_a of 6.6. Hence, the pK_a of phenolic hydroxyl group of JB2-48 (in the enzyme bound form) remains unresolved from that given by the protonation/deprotonation of the sulfonamide moiety. It should be reiterated that the sulfonamide moiety of dansylamide fluorophore (which is devoid of the phenolic hydroxyl group) also shows the pK_a of 6.3 when bound to hCA I [34]. Irrespectively, a comparative account of the pK_a values of JB2-48 in free and the enzyme bound forms clearly attests to the fact that the sulfonamide as well as phenolic hydroxyl groups of the enzyme bound fluorophore remain fully protonated and deprotonated (ionized) at pH values 5.0 and 9.0, respectively, and at these pH extrema, the enzyme bound fluorophore exhibits minimum and maximum fluorescence intensities, respectively.

In view of the above information, we could probe the contributions of hydrophobic versus electrostatic interactions in the ground and putative transition states upon binding of JB2-48 to hCA I, respectively (see below). Fig. 3 shows the emission spectra of hCA I ($\lambda_{\text{ex}} = 280 \text{ nm}$) in the presence of increasing concentrations of JB2-48 at pH 7.0. We ascribe the intrinsic fluorescence of hCA I to the enzyme resident tryptophan residues. As shown in Fig. 3A, as the concentration of JB2-48 increases, whereas the fluorescence emission intensity of the tryptophan residues ($\lambda_{\text{em}} = 330 \text{ nm}$) decreases (presumably due to the static quenching), the emission intensity of the probe ($\lambda_{\text{em}} = 470 \text{ nm}$) increases. Given the changes in fluorescence signals at the above wavelengths, we titrated a fixed concentration of hCA I by increasing concentrations of the fluorophore to determine the binding constant of the enzyme–fluorophore complex. Fig. 3B shows the titration profiles for the binding of JB2-48 with hCA I, obtained by monitoring the intrinsic fluorescence of the enzyme (decrease in the fluorescence intensity at 330 nm; open circles) as well as the probe's signal (increase in the fluorescence at 470 nm; open triangle). The solid smooth lines are the best fit of the data for the dissociation constants of

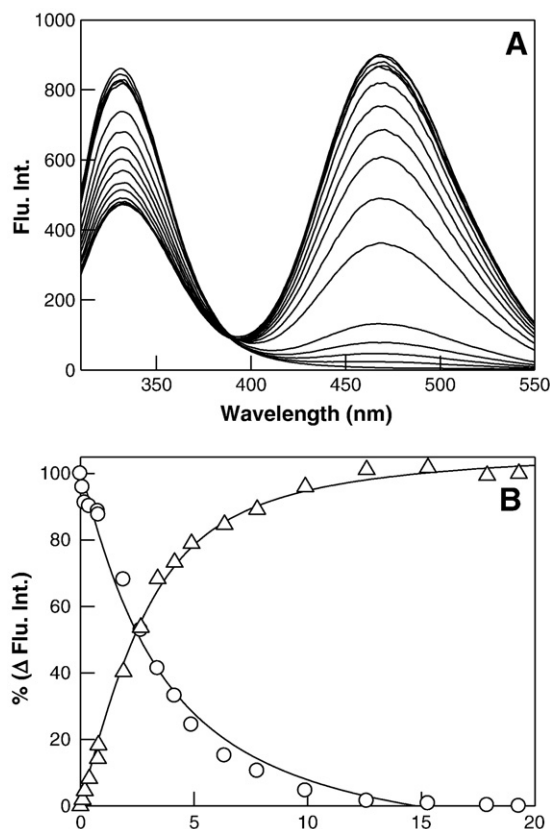


Fig. 3. Fluorescence spectral changes and binding isotherms for the interaction of JB2-48 with hCA I. Panel A shows the fluorescence emission spectra of hCA I in the absence and presence of increasing concentrations of JB2-48. [hCA I] = 2 μM . The concentration of [JB2-48] for the emission spectra (low to high fluorescence emission intensity at 470 nm region) has been 0, 0.1, 0.2, 0.4, 0.78, 1.9, 2.7, 4.2, 4.9, 6.3, 7.8, 9.9, 12.6, 15.3, 17.9, 19.3 μM , respectively; $\lambda_{\text{ex}} = 280 \text{ nm}$. Note that the titration of hCA I by JB2-48 results in a decrease in the fluorescence intensity at 330 nm, and increase in the fluorescence intensity at 470 nm. Panel B shows the binding isotherms for the interaction of JB2-48 with hCA I determined at 330 nm (\circ ; decreasing phase) and at 470 nm (Δ ; increasing phase). $\lambda_{\text{ex}} = 280 \text{ nm}$; hCA I = 2 μM . The solid smooth lines are the best fit of the data for the K_d values of 2.1 ± 0.2 (330 nm plot) and $2.3 \pm 0.4 \mu\text{M}$ (470 nm plot), respectively.

the enzyme–probe complex as being equal to 2.1 ± 0.2 and $2.3 \pm 0.4 \mu\text{M}$ at 325 and 470 nm, respectively, at pH 7.0. We further determined the K_i value of JB2-48 using p-nitriphenyl acetate as the enzyme substrate as described by Banerjee et al. [42] and found its magnitude to be $2.7 \pm 0.5 \mu\text{M}$. Note that all these values are comparable, and thus they appear to originate from a common physical/binding step. We performed similar experiment to determine the binding affinity of JB2-48 for hCA I at pH 5.0 and 9.0, respectively. In these experiments, the concentration of JB2-48 was increased until the enzyme appeared to be nearly saturated. These values are summarized in Table 1. Using the standard state as being equal to 1.0 M and pH = 7.0, we translated the K_d values of Table 1 to the standard free energy changes (ΔG°) for the

Table 1
Binding of JB2-48 to hCA I as a function of pH^a.

pH	K_d	ΔG° ^b
5.0	6.0 μM	−7.1 kcal/mol
7.0	2.2 μM	−7.7 kcal/mol
9.0	0.14 μM	−9.3 kcal/mol

^a The concentrations of hCA I and JB2-48 at different pH values were as follows: pH 5.0: [hCA I] = 3.0 μM , [JB2-48] = 0–35.8 μM pH 7.0: [hCA I] = 2 μM , [JB2-48] = 0–19.3 μM pH 9.0: [hCA I] = 3 μM , [JB2-48] = 0–7.2 μM .

^b The standard state of pH was taken as 7.0 in computing the ΔG° values.

enzyme–ligand interactions at 25 °C ($\Delta G^\circ = -RT \ln (1/K_d)$), and these derived values are presented as the last column of Table 1. A casual perusal of the ΔG° values of Table 1 reveals that the difference in the enzyme–JB2-48 binding energy ($\Delta\Delta G^\circ$) between the high and low pH values is 2.2 kcal/mol. Since at the above high and low pH values, the sulfonamide nitrogen of JB2-48 is expected to exist in fully ionized and neutral forms, respectively, the calculated $\Delta\Delta G^\circ$ value serves to be the measure of the electrostatic energetic contribution between the active site resident Zn^{2+} cofactor and the negatively charged sulfonamide moiety of the fluorophore.

3.1. Effects of solvent polarity and the enzyme's active site microenvironment on the steady-state and fluorescence lifetimes of JB2-48

Both structural as well as isothermal titration microcalorimetric (ITC) data for the binding of ligands to hCA I revealed that the active site pocket of the enzyme is predominantly hydrophobic [17,28]. To probe as to the extent such hydrophobicity modulates the fluorescent properties of the enzyme bound JB2-48, we determined the emission maxima ($\lambda_{ex} = 330$ nm) and lifetimes of the fluorophore in the presence of increasing concentration (from 0 to 90%) of dioxane. Since we used 10% DMSO to solubilize the fluorophore, we could maintain the concentration of dioxane between 0% and 90%. As shown in Table 2, as the concentration of dioxane increases, the fluorescence emission maxima of JB2-48 progressively shifts to blue. We further observed that at all concentrations of dioxane, the excited state decay profile of JB2-48 ($\lambda_{ex} = 340$ nm, $\lambda_{em} = 470$ nm; see Experimental procedures) conforms to the single lifetime with increasing magnitude as a function of the dioxane concentration. This feature is consistent with our previous observation [38] that the fluorescence emission intensity of the fluorophore increases with increase in dioxane concentration. It should be pointed out that due to solubility problem, we could not reliably perform the above experiment in different solvents to ascertain the contributions of hydrogen bonding and/or other microenvironment effect on the spectral features of JB2-48.

We attempted to ascertain what concentration of dioxane qualitatively mimics the hydrophobicity of the enzyme's active site pocket. In this endeavor, we determined the fluorescence lifetimes of the enzyme bound JB2-48 at neutral (pH 7.0), acidic (pH 5.0), and alkaline (pH 9.0) pH values (Fig. 4). By coincidence, we noted that the fluorescence lifetime of JB2-48 in 90% dioxane (12.5 ± 0.1 ns; Table 2) was similar to the shorter lifetime of the enzyme bound fluorophore at pH 7.0 (see below). In Fig. 4, we show a comparative account of fluorescence decay profiles of JB2-48 in the presence of 90% dioxane (panel A), and JB2-48 bound to hCA I at pH 7.0 (panel B), pH 5.0 (panel C), and pH 9.0 (panel D). The solid smooth lines are the best fit of the data for one (panels A, B, and D) or two (panel B) lifetimes of the fluorophores; the residuals of the fitted data are shown at the bottom of the individual panel. A comparison of the lifetime data of Fig. 4A and B revealed that unlike the excited state decay profile of JB2-48 in the presence of 90% dioxane (conforming to the single lifetime profile

of 12.5 ns), the hCA I bound form of the fluorophore at pH 7.0 yields two lifetimes of 13.5 and 27.3 ns, respectively. Clearly, JB2-48 does not experience identical microscopic environment in 90% dioxane vis a vis that present at the active site pocket of hCA I at the neutral pH. However, since the shorter lifetime of the fluorophore in the presence of the enzyme (13.5 ns) is similar to that observed in the presence of 90% dioxane (12.5 ns), we surmise that the shorter lifetime component is given by the microscopic state of the enzyme which harbors the protonated (i.e., non-ionic) form of the sulfonamide moiety of JB2-48 (see Discussion). To test this hypothesis, we compared the lifetime profiles of hCA I–JB2-48 complex at neutral pH with those determined at low (pH=5.0; Fig. 4C) and high pH (pH=9.0; Fig. 4D) values. Such comparison revealed that unlike at neutral pH, the excited state fluorescence decay traces at low and high pH values conformed to single lifetimes with magnitudes of 14 and 20 ns, respectively. Note that the latter values are similar to the shorter (13.5 ns) and longer (27.3 ns) lifetime components for the excited state decay data of the enzyme bound JB2-48 at pH 7.0 (Fig. 4B). Evidently, the prevalence of two lifetimes of the enzyme bound JB2-48 at the neutral pH, but single lifetimes at lower and higher pH values imply that ionized and neutral forms of sulfonamide moiety of JB2-48 are stabilized by the corresponding microscopic states of the enzyme. In one such state, the fluorescence properties of the enzyme bound JB2-48 is primarily given by the ligand harboring the neutral form of sulfonamide (i.e., at pH 5.0), where in the other state it is given by the negatively charged sulfonamide moiety (i.e., at pH 9.0) of the ligand.

3.2. Effect of temperature on the fluorescence lifetimes of free and enzyme bound JB2-48

Although our above experimental data led to the suggestion that the differential fluorescence profiles (including lifetimes) of JB2-48 under different environmental conditions were contributed by the hydrophobic and electrostatic interactions within the active site pocket of hCA I, we did not rule out the possibility that such changes originated from the restriction in rotational freedom between the two aromatic rings of the fluorophore as delineated in the case of green fluorescent protein [43]. However, such possibility seemed unlikely since both parent fluorophore (dansylamide) as well as its different derivatives [38] showed increase in fluorescence as well as the blue shift in their emission maxima. In addition, our pK_a measurement of free JB2-48 (Fig. 2B) reveals that the phenolic hydroxyl group yields an unusually low pK_a (6.5 instead of 10 for phenol) value, presumably because of delocalization of the electrons (formed upon deprotonation of the phenolic hydroxyl group) via extended conjugation between the two aromatic rings as well as the terminal sulfonamide moiety. Hence, even the aqueous form of JB2-48 (at least at neutral and basic pH values) is likely to be devoid of the rotational freedom as noted with the individual fluorophoric units of green fluorescent protein [43]. To substantiate or refute this conclusion, we determined the fluorescence lifetimes of free JB2-48 as well as its enzyme bound form at pH 7.0 as a function of temperature. As shown in Table 3, the increase in temperature from 25 to 40 °C (the range where enzyme remains fully active) has practically no effect on the lifetimes of either free or the enzyme bound JB2-48. Hence, the enhancement in the fluorescence intensity of JB2-48 is not due to restriction in the rotational freedom (enhancing internal conversion) around the “bridged atoms” connecting the two aromatic rings of the fluorophore upon binding to the enzyme.

3.3. Transient kinetic studies for the binding of JB2-48 to hCA I

We performed transient kinetic studies for the binding of JB2-48 to hCA I at pH 5.0 and 9.0, respectively. This was accomplished by mixing the above species via the stopped flow syringes, followed by

Table 2
Fluorescence emission maxima and lifetimes of JB2-48 in dioxane^a.

% Dioxane	Emission maxima (nm)	Lifetime (ns)
0	528	1.2±0.02
25	522	2.4±0.05
50	515	4.9±0.09
75	nd	8.4±0.1
90	494	12.5±0.1

^a All solutions contained 10% DMSO. $\lambda_{ex} = 336$ for determining emission maxima and 340 nm (LED source) for determining lifetimes. nd—not determined.

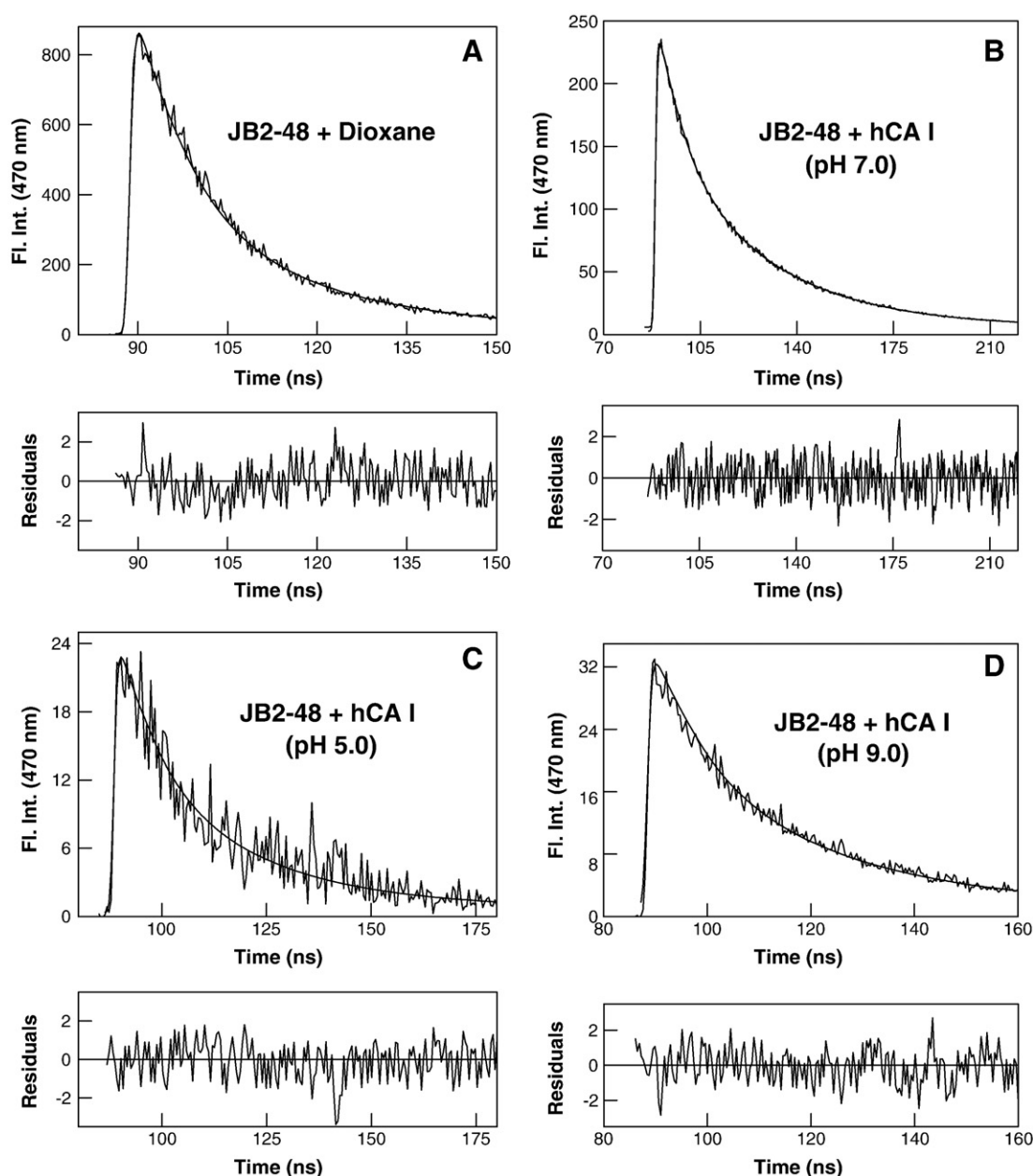


Fig. 4. Time-resolved excited state decay profiles of JB2-48 in the presence of dioxane as well as hCA I at different pH values. The time courses for the decay of the excited state of 4 μM JB2-48 ($\lambda_{\text{ex}} = 340 \text{ nm}$, $\lambda_{\text{em}} = 470 \text{ nm}$) in the presence of 90% dioxane (Panel A) and 50 μM hCA I at different pH values (Panels B–D) The solid smooth lines are the best fit of the data for one (Panels A, C, and D) and two (Panel B) lifetimes (τ) under different experimental conditions. Panel A (90% dioxane) $\tau = 12.5 \pm 0.1 \text{ ns}$, Panel B (hCA I, pH 7.0) $\tau_1 = 13.5 \pm 0.1 \text{ ns}$, $\tau_2 = 27.3 \pm 0.4 \text{ ns}$, Panel C (hCA I, pH 5.0) $\tau = 14 \pm 0.6 \text{ ns}$, and Panel D (hCA I, pH 9.0) $\tau = 20 \pm 0.7 \text{ ns}$. The residuals of the fitted data are given at the bottom of the lifetime traces of the individual panel.

monitoring the increase in fluorescence intensity of the probe ($\lambda_{\text{ex}} = 336 \text{ nm}$, cutoff filter = 395 nm) as a function of time. Fig. 5

Table 3
Effect of temperature on lifetimes of JB2-48^a.

Temperature (°C)	Free JB2-48	hCA I–JB2-48 complex	
	τ (ns)	τ_1 (ns)	τ_2 (ns)
25	1.2 ± 0.02	13.5 ± 0.1	27.3 ± 0.4
30	1.3 ± 0.03	12.7 ± 0.004	29.1 ± 0.01
35	1.3 ± 0.03	11.6 ± 0.1	28.6 ± 0.01
40	1.2 ± 0.03	12.8 ± 0.2	28.7 ± 0.3

^a In 25 mM HEPES buffer, pH 7.0, containing 10% DMSO. $\lambda_{\text{ex}} = 340 \text{ nm}$ (LED) and $\lambda_{\text{em}} = 470 \text{ nm}$. [JB2-48] = 35 μM for measuring the lifetimes of free fluorophore. [JB2-48] = 4 μM and [hCA I] = 50 μM for measuring the lifetimes of the enzyme bound fluorophore.

shows the stopped flow traces for the binding of JB2-48 with hCA I under pseudo-first order condition ($[\text{JB2-48}] \gg [\text{hCA I}]$) at the above pH values. The solid smooth lines are the best fit of the data for the single exponential rate equation with rate constants of 0.08 and 0.37 s^{-1} at pH 5.0 and 9.0, respectively. These rate constants are translated into the activation energies ($\Delta G^{\ddagger} = -RT \ln(6.2 \times 10^{12}/k)$) of 18.9 and 18.0 kcal/mol at the above pH values, respectively. In view of our earlier argument, the difference in the putative transition state energies ($\Delta \Delta G^{\ddagger} = 0.9 \text{ kcal/mol}$) for the binding of JB2-48 to hCA I between pH 5.0 and 9.0 serve as the quantitative measure of the electrostatic contribution (involving the negatively charged sulfonamide group of JB2-48 and the Zn^{2+} cofactor) in stabilizing the ligand in the transition state.

To further confirm that the magnitude (as well as the associated transient rate constants) of fluorescence changes for the binding of

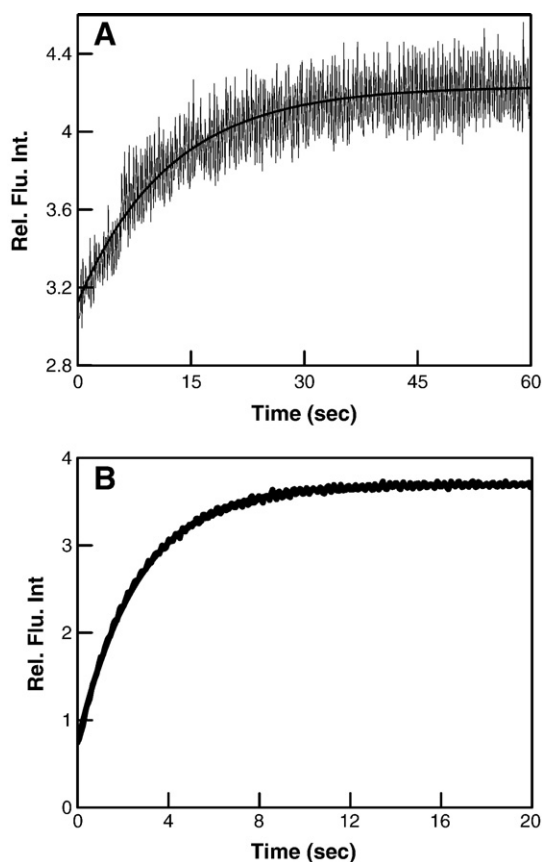


Fig. 5. Transient kinetics for the binding of JB2-48 to hCA I at acidic and basic pH values. The stopped flow traces for the mixing of JB2-48 with hCA I ($\lambda_{\text{ex}} = 336$ nm, “cutoff” filter = 395 nm) at pH 5.0 and 9.0 are shown in Panels A and B, respectively. The after-mixing concentrations of hCA I and JB2-48 were 1 and 30 μM , respectively. The solid smooth lines are the best fit of the data according to the single exponential rate equation for the relaxation rate constants (k_{obs}) of 0.08 ± 0.004 and 0.37 ± 0.001 s^{-1} at pH 5.0 and 9.0, respectively.

JB2-48 to hCA I between the low (Fig. 5A) and high (Fig. 5B) pH values were given by the neutral versus the ionized forms of the sulfonamide moiety of the ligand, respectively, we performed the “pH jump” experiment. In this endeavor, we mixed hCA I–JB2-48 complex present in 5 mM Tris buffer at pH 9.0 with 200 mM acetate buffer at pH 5.0 (the pH of the mixture emerged out to be 5.0) via the stopped flow syringes, and monitored the time course of the fluorescence changes. Fig. 6 shows the time dependent decrease in fluorescence of the hCA I–JB2-48 complex upon pH jump from 9 to 5. An essentially identical experiment was performed for the mixing of hCA I–JB2-48 complex maintained at pH 5.0 with 200 mM Tris buffer of pH 9.0 (the pH of the mixture was 9.0). Note that the opposite pH jump (i.e., from 5.0 to 9.0) resulted in the time dependent increase (Fig. 6) in fluorescence of the enzyme–probe complex. Both the traces of Fig. 6 conformed to the single exponential rate equation with rate constants of 0.078 and 0.67 s^{-1} for the pH jump from 9 to 5 and that from 5 to 9, respectively. On the basis that the protonation/deprotonation reactions are diffusion limited [40], the origin of the above rate constants must lie in the slow change in the electronic structure of the hCA I bound JB2-48, which is likely to originate from the readjustment/packing of the enzyme–ligand complex. This is further supported by the fact that the transient rate constants for the association of JB2-48 to hCA I at pH 5.0 and 9.0 (Fig. 5) are comparable to those obtained from the pH jump experiments from 9 to 5 and from 5 to 9 (Fig. 6), respectively (see Discussion).

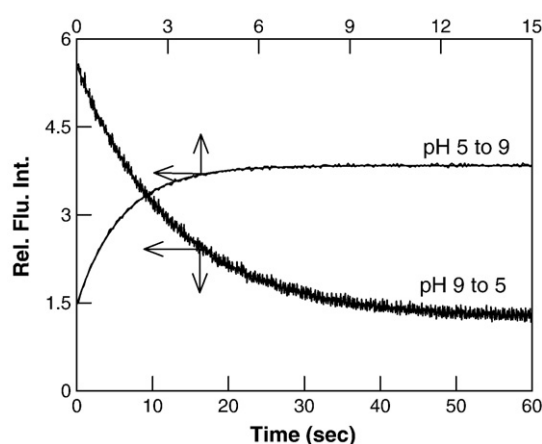


Fig. 6. pH jump relaxation kinetic studies of hCA I bound JB2-48. The stopped-flow traces for the change in fluorescence of the hCA I–JB2-48 complex upon mixing (the after mixing concentrations of hCA I and JB2-48 being equal to 1 μM and 20 μM , respectively) with buffers of selected pH values are shown. The pH jump from 5 to 9 (increase in fluorescence) was accomplished by mixing the hCA I–JB2-48 complex in 5 mM acetate buffer (pH 5.0) with 200 mM Tris buffer (pH 9.0). The pH of the mixture was found to be 9.0. The pH jump from 9 to 5 (decrease in fluorescence) was accomplished by mixing the hCA I–JB2-48 complex in 5 mM Tris buffer (pH 9.0) with 200 mM acetate buffer (pH 5.0). The pH of the mixture was found to be 5.0. The solid smooth lines are the best fit of the data according to the single-exponential rate equation with the rate constants of 0.67 ± 0.003 s^{-1} and 0.078 ± 0.0005 s^{-1} for the pH jump experiments from 5 to 9 and from 9 to 5, respectively.

4. Discussion

The experimental data presented in the previous section lead to the following conclusions: (1) Due to its size and extended conjugation, JB2-48 occupies nearly the entire active site pocket (about 15 Å deep) of hCA I, and this feature allows for deciphering the hydrophobic versus electrostatic contributions on the spectral, kinetic, and thermodynamic features of the enzyme–ligand complex. (2) Whereas the pK_a of sulfonamide moiety of free JB2-48 is 10.2 that of the phenolic hydroxyl group is 6.5. (3) Depending upon the pH of the buffer media, the enzyme bound JB2-48 exists in either neutral (with sulfonamide group being fully protonated) or anionic form ($\text{pK}_a = 6.6$), and these forms are stabilized by the cognate microscopic states of the enzyme. (4) The neutral and anionic forms of the enzyme bound JB2-48 are distinguishable by their fluorescent lifetimes; whereas the fluorescent lifetime of the neutral form falls in the range of 12–14 ns, that of the anionic form is greater than 20 ns. Consistently, the anionic form of the enzyme bound JB2-48 is more fluorescent than its neutral counterpart. (5) Due to added electrostatic interaction (between the enzyme resident Zn^{2+} cofactor and the negatively charged sulfonamide group), the anionic form of JB2-48 is stabilized at the active site of hCA I by about 2.2 kcal/mol energy than its neutral form. (6) The rate of fluorescence changes accompanying the transient course of binding of JB2-48 to hCA I is about 5 fold faster with anionic than neutral form of the ligand, unraveling the fact that the putative transition state is about 0.9 kcal/mol more favorable with the anionic form of the ligand than the neutral form. (7) The similarity in the rate constants for the association of JB2-48 with hCA I (at acidic and basic pH values) with those derived from the pH jump experiments lead to the suggestion that the active site pocket of the enzyme undergoes slow restructuring during the course of the ligand binding.

This is the first demonstration (to the best of our knowledge) that the fluorescence spectral changes upon binding of JB2-48 to hCA I is contributed both by the hydrophobic environment of the enzyme’s active site pocket as well as the electrostatic interaction between the active site resident Zn^{2+} cofactor and the negatively charged sulfonamide group of the ligand. Our temperature dependent lifetime data of both free and the enzyme bound JB2-48 (Table 3) as well as the

pK_a values of free fluorophore eliminates the possibility that the enhancement in fluorescence of JB2-48 (upon binding to the enzyme site) is due to restriction in the rotational freedom between the two aromatic rings as observed with green fluorescent protein [43]. We believe the fluorescence changes upon binding of JB2-48 (vis a vis dansylamide; [34]) to hCA I is more pronounced due to an extended conjugation of the π electrons between the two aromatic rings. The fact that the fluorescence intensity of JB2-48 increases with decrease in the solvent polarity [38] attests to the contribution of the hydrophobic active site environment of hCA I in enhancing the fluorescence emission intensity of the ligand. However, since the fluorescence emission intensity of the enzyme bound JB2-48 is significantly higher at neutral and basic pH values (as compared to that obtained in the presence of 90% dioxane) implies that aside from hydrophobicity, some additional factor(s) of the enzyme site phase is involved in enhancing the fluorescence intensity of the ligand. Based on the structural as well as the spectroscopic data [18–20,26,27,30], it appeared evident that such an “additional factor” is the electrostatic interaction between the active site resident Zn^{2+} and the negatively charged sulfonamide group of the ligand. Hence, it is not surprising that the decrease in pH diminishes the fluorescence emission intensity of the enzyme bound JB2-48 (Fig. 2).

In view of the fact that the pK_a value of the enzyme bound JB2-48 is equal to 6.6, it is conceivable that the enzyme bound form of the above ligand would remain in fully protonated and ionized states at pH 5 and 9, respectively. This feature is further corroborated by the lifetime measurements of JB2-48 under different experimental conditions (Fig. 4). Since the lifetime of “free” JB2-48 in 90% dioxane ($\tau = 12.5$ ns) is similar to the lifetime of the enzyme bound JB2-48 at pH 5.0 ($\tau = 14$ ns), it supports the notion (rather quantitatively) that the fluorescence profile of the enzyme bound ligand at $pH < pK_a$ is dominated by the hydrophobic interaction within the enzyme's active site pocket. This is in contrast to the lifetime of the enzyme bound JB2-48 at pH 9.0 being equal to 20 ns (Table 1), supports our hypothesis that at $pH > pK_a$, the fluorescence profile of the enzyme bound ligand is contributed by a combination of hydrophobic and electrostatic interactions. Hence, it is not surprising that at pH 7.0 (i.e., $pH \approx pK_a$), the enzyme bound JB2-48 yields two lifetimes of 13.5 ns (τ_1) and 27.3 ns (τ_2), of which τ_1 and τ_2 are similar to the lifetimes of the enzyme bound ligand at pH 5.0 (or the free ligand in the presence of 90% dioxane) and at pH 9.0, respectively. Since under physiological conditions CAs are known to bind one molecule of arylsulfonamide ligand per monomeric unit of the enzyme [15,17–22,28,29,41], it appears plausible that τ_1 and τ_2 are associated with the two alternative microscopic states of the enzyme (see the cartoon of Fig. 7).

The question arose whether the two microscopic states of the hCA I, harboring neutral versus anionic forms of JB2-48, respectively, are representative of the alternative conformational states of the

enzyme. In pursuit of answering this question, we note that the observed rate constants during the pH jump experiments (Fig. 6) are several orders of magnitude lower than those expected for the simple protonation/deprotonation (which are considered to be the diffusion limited process; 49) step of the sulfonamide group of the enzyme bound ligand. Evidently, the protonation/deprotonation of the enzyme-bound ligand may not be the rate limiting step of the fluorescence changes during the pH jump experiments. The overall rate is neither expected to be contributed by the rate of decay of the excited state of the enzyme bound fluorophores since the lifetimes of the enzyme bound JB2-48 falls in the range of nanoseconds. However, one can argue that the slower rate constant for the increase in the fluorescence of the enzyme bound JB2-48, particularly during the 9 \rightarrow 5 pH jump experiment ($k_{obs} = 0.08$ s $^{-1}$), is due to slow (rate limiting) breakdown of the Zn^{2+} - (anionic) sulfonamide bond of the ligand prior to the diffusion limited protonation step. Unfortunately, the above possibility falls short in explaining the comparably lower rate of fluorescence changes ($k_{obs} = 0.67$ s $^{-1}$) during the 5 \rightarrow 9 pH jump experiment. Aside from these, the observed rate constants for the association of JB2-48 to hCA I at pH 5 ($k_{obs} = 0.08$ s $^{-1}$) and 9 ($k_{obs} = 0.37$ s $^{-1}$) (Fig. 5) are similar to the rate constants for the 9 \rightarrow 5 and 5 \rightarrow 9 pH jump experiments, respectively. Such a similarity in the rate constants has been somewhat surprising since these experiments are mechanistically different. In one case, the transient course of the fluorescence changes (as a function of pH) occur due to the association of the ligand to the enzyme, but in other case, the overall process is manifested via the protonation/deprotonation of the enzyme bound ligand. These arguments, in conjunction with our earlier transient kinetic studies for the binding of dansylamide to hCA I and hCA II [34], prompt us to propose that the two alternative microscopic states of the hCA I (Fig. 7) are representative of two alternative conformational states of the enzyme which stabilize neutral and anionic forms of the ligand, and the transition between the above states serve as the rate limiting step during the pH dependent experiments. It should be emphasized that the conformational changes during the ligand binding and/or the pH jump experiments need not be extensive to be deciphered via the fluorescence techniques—they can just be subtle and/or dynamic in nature to elicit the fluorescence changes reported herein.

The mechanistic conclusion derived herein has potential to find applications in the rationale design of hCA inhibitors as therapeutic agents. It appears evident that the potency of an arylsulfonamide inhibitor of hCAs can be increased by incorporating non polar groups toward the exterior region of the active site pocket as well as by introducing the electronic withdrawing groups on the aromatic ring (s) of the inhibitor [13,14,28,31–33]. The latter groups would facilitate the deprotonation of the sulfonamide moiety (of the inhibitor) such that it's anionic form would interact more strongly with the Zn^{2+} cofactor, and the overall structure would be stabilized by the cognate

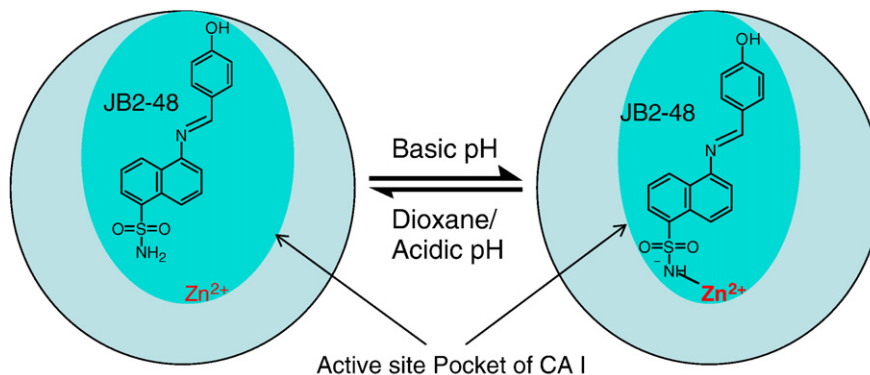


Fig. 7. Cartoon showing the stabilization of neutral and anionic forms of JB2-48 at complementary microscopic states of hCA I. The factors affecting the reversible transition between the two forms of the enzyme–ligand complexes are shown.

microscopic/conformational state of the enzyme. As long as the newly incorporated groups do not pose steric hindrance within the active site pocket of the enzyme, nor do they alter the formal charges on the Zn²⁺ cofactor, the resultant inhibitors would exhibit high potencies. On the other hand, any factor which impairs deprotonation of the sulfonamide moiety would populate the other conformational state of the enzyme with weaker inhibitory potency. We are currently testing the above hypothesis by rationally designing the new sets hCA inhibitors, and we will report these findings subsequently.

Acknowledgments

This research was supported by the NIH grants CA113746 and CA132034 and the National Science Foundation grant DMR-0705767 to D.K.S and S.M. Sumathra Manokaran was supported by the National Science Foundation—Experimental Program to Stimulate Competitive Research Award [grant number EPS-0814442].

References

- [1] H. Ke, H. Wang, Crystal structures of phosphodiesterases and implications on substrate specificity and inhibitor selectivity, *Curr. Top. Med. Chem.* 7 (2007) 391–403.
- [2] J. Ren, R. Esnouf, E. Garman, D. Somers, C. Ross, I. Kirby, J. Keeling, G. Darby, Y. Jones, D. Stuart, High resolution structures of HIV-1 RT from four RT-inhibitor complexes, *Nat. Struct. Biol.* 2 (1995) 293–302.
- [3] B.M. Dunn, S. Hung, The two sides of enzyme–substrate specificity: lessons from the aspartic proteinases, *Biochim. Biophys. Acta* 1477 (2000) 231–240.
- [4] H.A. Carlson, Protein flexibility and drug design: how to hit a moving target, *Curr. Opin. Chem. Biol.* 6 (2002) 447–452.
- [5] C.F. Wong, J.A. McCammon, Protein flexibility and computer-aided drug design, *Annu. Rev. Pharmacol. Toxicol.* 43 (2003) 31–45.
- [6] S.J., Teague Implications of protein flexibility for drug discovery, *Nat. Rev. Drug Discov.* 2 (2003) 527–541.
- [7] C.F. Wong, A.J. McCammon, Protein simulation and drug design, *Adv. Protein Chem.* 66 (2003) 87–121.
- [8] A.M. Davis, S.J. Teague, G.J. Kleywegt, Applications and limitations of X-ray crystallographic data in structure-based ligand and drug design, *Angew. Chem. Int. Ed.* 42 (2003) 2718–2736.
- [9] N. Neamati, J.J. Barchi Jr., New paradigms in drug design and discovery, *Curr. Top. Med. Chem.* 2 (2002) 211–227.
- [10] W.R. Chegwidden, N.D. Carter, The carbonic anhydrases: new horizons, Birkhauser Verlag, Basel, Switzerland, 2000.
- [11] W.S. Sly, P.Y. Hu, Human carbonic anhydrases and carbonic anhydrase deficiencies, *Annu. Rev. Biochem.* 64 (1995) 375–401.
- [12] R.E. Tashian, Genetics of the mammalian carbonic anhydrases, *Adv. Genet.* 30 (1992) 321–356.
- [13] C.T. Supuran, A. Scozzafava, A. Casini, Carbonic anhydrase inhibitors, *Med. Res. Rev.* 23 (2003) 146–189.
- [14] C.T. Supuran, A. Scozzafava, J. Conway, Carbonic anhydrase—its inhibitors and activators, CRC Press, Boca Raton, New York, 2004, pp. 1–363.
- [15] V.M. Krishnamurthy, G.K. Kaufman, A.R. Urbach, I. Gitlin, K.L. Gudiksen, D.B. Weibel, G.M. Whitesides, Carbonic anhydrase as a model for biophysical and physical-organic studies of proteins and protein–ligand binding, *Chem. Rev.* 108 (2008) 946–1051.
- [16] D.N. Silverman, R. McKenna, Solvent-mediated proton transfer in catalysis by carbonic anhydrase, *Acc. Chem. Res.* 40 (2007) 669–675.
- [17] K.K. Kannan, M. Ramanadham, T.A. Jones, Structure, refinement and function of carbonic anhydrase isozymes: refinement of human carbonic anhydrase I, *Ann. N.Y. Acad. Sci.* 429 (1984) 49–60.
- [18] A.E. Eriksson, T.A. Jones, A. Liljas, Refined structure of human carbonic anhydrase II at 2.0 Å resolution, *Proteins Struct. Funct. Genet.* 4 (1988) 274–282.
- [19] D.M. Duda, C. Tu, S.Z. Fisher, H. An, C. Yoshioka, L. Govindasamy, P.J. Laipis, M. Aqbandje-McKenna, D.N. Silverman, R. McKenna, Human carbonic anhydrase III: structural and kinetic study of catalysis and proton transfer, *Biochemistry* 44 (2005) 10046–10053.
- [20] T. Stams, S.K. Nair, T. Okuyama, A. Waheed, W.S. Sly, D.W. Christianson, Crystal structure of the secretory form of membrane-associated human carbonic anhydrase IV at 2.8-Å resolution, *Proc. Natl. Acad. Sci. USA* 93 (1996) 13589–13594.
- [21] P.A. Boriack-Sjodin, R.W. Heck, P.J. Liaipis, D.N. Silverman, D.W. Christianson, Structure determination of murine mitochondrial carbonic anhydrase V at 2.45-Å resolution: implications for catalytic proton transfer and inhibitor design, *Proc. Natl. Acad. Sci. USA* 92 (1995) 10949–10953.
- [22] D.A. Whittington, A. Waheed, B. Ulmasov, G.N. Shah, J.H. Grubb, W.S., D.W. Christianson, Crystal structure of the dimeric extracellular domain of human carbonic anhydrase XII, a biotopic membrane protein overexpressed in certain cancer tumor cells, *Proc. Natl. Acad. Sci. USA* 98 (2001) 9545–9550.
- [23] V. Alterio, M. Hilvo, A. DiFlore, C.T. Supuran, P. Pan, S. Parkkila, A. Scaloni, J. Pastorek, S. Pastorekova, C. Pedone, A. Scozzafava, S.M. Monti, G. De Simone, Crystal structure of the catalytic domain of the tumor-associated human carbonic anhydrase IX, *Proc. Natl. Acad. Sci. USA* 106 (2009) 16233–16238.
- [24] B.C. Tripp, K. Smith, J.G. Ferry, Carbonic anhydrase: new insights for an ancient enzyme, *J. Biol. Chem.* 276 (2001) 48615–48618.
- [25] K.K. Kannan, B. Notstrand, K. Fridborg, S. Lovgren, A. Ohlsson, M. Petef, Crystal structure of human erythrocyte carbonic anhydrase B. Three dimensional structure at a nominal 2.2-Å resolution, *Proc. Natl. Acad. Sci. USA* 72 (1975) 51–55.
- [26] G.M. Blackburn, B.E. Mann, B.F. Taylor, A.F. Worrall, A nuclear magnetic resonance study of the binding of novel N-hydroxybenzenesulfonamide carbonic anhydrase inhibitors to native and cadmium-111 substituted carbonic anhydrase, *Eur. J. Biochem.* 153 (1985) 553–558.
- [27] K. Kanamori, J.D. Roberts, Nitrogen-15 nuclear magnetic resonance study of benzenesulfonamide and cyanate binding to carbonic anhydrase, *Biochemistry* 22 (1983) 2658–2664.
- [28] D.K. Srivastava, K.M. Jude, A.L. Banerjee, M. Haldar, S. Manokaran, J. Kooren, S. Mallik, D.W. Christianson, Structural analysis of charge discrimination in the binding of inhibitors to human carbonic anhydrases I and II, *J. Am. Chem. Soc.* 129 (2007) 5528–5537.
- [29] K.M. Jude, A.L. Banerjee, M.K. Haldar, S. Manokaran, B. Roy, S. Mallik, D.K. Srivastava, D.W. Christianson, Ultrahigh resolution crystal structures of human carbonic anhydrases I and II complexed with “two-prong” inhibitors reveal the molecular basis of high affinity, *J. Am. Chem. Soc.* 128 (2006) 3011–3018.
- [30] J.E. Coleman, Chemical reactions of sulfonamides with carbonic anhydrase, *Ann. Rev. Pharmacol.* 15 (1975) 221–242.
- [31] S.P. Gupta, Quantitative structure–activity relationships of carbonic anhydrase inhibitors, *Prog. Drug Res.* 60 (2003) 171–204.
- [32] A. Vedani, E.F. Meyer Jr., Structure–activity relationships of sulfonamide drugs and human carbonic anhydrase C: modeling of inhibitor molecules into the receptor site of the enzyme with an interactive computer graphics display, *J. Pharm. Sci.* 73 (1984) 352–358.
- [33] M.C. Menziani, P.G. DeBenedetti, F. Gago, W.G. Richards, The binding of benzenesulfonamides to carbonic anhydrase enzyme. A molecular mechanics study and quantitative structure–activity relationships, *J. Med. Chem.* 32 (1989) 951–956.
- [34] A.L. Banerjee, S. Tobwala, B. Ganguly, S. Mallik, D.K. Srivastava, Molecular basis for the origin of differential spectral and binding profiles of dansylamide with human carbonic anhydrase I and II, *Biochemistry* 44 (2005) 3673–3682.
- [35] R.F. Chen, J.C. Kernohan, Combination of bovine carbonic anhydrase with a fluorescent sulfonamide, *J. Biol. Chem.* 242 (1967) 5813–5823.
- [36] C.A. Fierke, R.B. Thompson, Fluorescence-based biosensing of zinc using carbonic anhydrase, *Biomaterials* 14 (2001) 205–222.
- [37] R.B. Thompson, B.P. Maliwal, H.H. Zeng, Zinc biosensing with multiphoton excitation using carbonic anhydrase and improved fluorophores, *J. Biomed. Opt.* 5 (2000) 17–22.
- [38] J. Banerjee, M.K. Haldar, S. Manokaran, S. Mallik, D.K. Srivastava, New fluorescent probes for carbonic anhydrases, *Chem. Commun.* 26 (2007) 2723–2725.
- [39] L. Qin, D.K. Srivastava, Energetics of two-step binding of a chromophoric reaction product, *trans*-3-indoleacryloyl-CoA, to medium chain acyl-CoA dehydrogenase, *Biochemistry* 37 (1998) 3499–3508.
- [40] G.G. Hammes, Thermodynamics and kinetics for the biological sciences, John Wiley & Sons Inc, New York, 2000.
- [41] S.K. Nair, D. Elbaum, D.W. Christianson, Unexpected binding mode of the sulfonamide fluorophore 5-dimethylamino-1-naphthalene sulfonamide to human carbonic anhydrase II. Implications for the development of a zinc biosensor, *J. Biol. Chem.* 71 (1996) 1003–1007.
- [42] A.L. Banerjee, M. Swanson, B.C. Roy, X. Jia, M. Haldar, S. Mallik, D.K. Srivastava, Protein surface-assisted enhancement in the binding affinity of an inhibitor for recombinant human carbonic anhydrase-II, *J. Am. Chem. Soc.* 126 (2004) 10875–10883.
- [43] R. Gepshtein, D. Huppert, N. Agmon, Deactivation mechanism of green fluorescent chromophore, *J. Phys. Chem. B* 110 (2006) 4434–4442.